

1 Exploration of PM_{2.5} sources on the regional scale in the 2 Pearl River Delta based on ME-2 modeling

3
4 Xiao-Feng Huang¹, Bei-Bing Zou¹, Ling-Yan He¹, Min Hu², André S. H. Prévôt³, Yuan-Hang
5 Zhang²

6 ¹Key Laboratory for Urban Habitat Environmental Science and Technology, School of
7 Environment and Energy, Peking University Shenzhen Graduate School, Shenzhen, 518055,
8 China.

9 ²State Key Joint Laboratory of Environmental Simulation and Pollution Control, College of
10 Environmental Sciences and Engineering, Peking University, Beijing, 100871, China.

11 ³Paul Scherrer Institute (PSI), 5232 Villigen-PSI, Switzerland.

12 13 **Abstract:**

14 The Pearl River Delta (PRD) of China, which has a population of more than 58 million people, is
15 one of the largest agglomerations of cities in the world and had severe PM_{2.5} pollution at the
16 beginning of this century. Due to the implementation of strong pollution control in recent decades,
17 PM_{2.5} in the PRD has continuously decreased to relatively lower levels in China. To
18 comprehensively understand the current PM_{2.5} sources in the PRD to support future air pollution
19 control strategy in similar regions, we performed regional-scale PM_{2.5} field observations coupled
20 with a state-of-the-art source apportionment model at six sites in four seasons in 2015. The
21 regional annual average PM_{2.5} concentration based on the 4-month sampling was determined to be
22 37 µg/m³, which is still more than three times the WHO standard, with organic matter (36.9%) and
23 SO₄²⁻ (23.6%) as the most abundant species. A novel multilinear engine (ME-2) model was firstly
24 applied to a comprehensive PM_{2.5} chemical dataset to perform source apportionment with
25 predetermined constraints, producing more environmentally meaningful results compared to those
26 obtained using traditional positive matrix factorization (PMF) modeling. The regional annual
27 average PM_{2.5} source structure in PRD was retrieved to be secondary sulfate (21%), vehicle
28 emissions (14%), industrial emissions (13%), secondary nitrate (11%), biomass burning (11%),
29 secondary organic aerosol (SOA, 7%), coal burning (6%), fugitive dust (5%), ship emissions (3%)
30 and aged sea salt (2%). Analyzing the spatial distribution of PM_{2.5} sources under different weather
31 conditions clearly identified the central PRD area as the key emission area for SO₂, NO_x, coal
32 burning, biomass burning, industrial emissions and vehicle emissions. It was further estimated that
33 under the polluted northerly air flow in winter, local emissions in the central PRD area accounted
34 for approximately 45% of the total PM_{2.5}, with secondary nitrate and biomass burning being most
35 abundant; in contrast, the regional transport from outside the PRD accounted for more than half of
36 PM_{2.5}, with secondary sulfate representing the most abundant transported species.

37
38 **Keywords:** source apportionment; ME-2; local emissions; regional transport; Pearl River Delta.

39 **1 Introduction**

40 With China's rapid economic growth and urbanization, air pollution has become a serious
41 problem in recent decades. Due to its smaller size, fine particulate matter (PM_{2.5}) can carry toxic
42 chemicals into human lungs and bronchi, causing respiratory diseases and cardiovascular diseases
43 that can harm human health (Sarnat et al., 2008; Burnett et al., 2014). In particular, long-term
44 exposure to high concentrations of fine particulate matter can also lead to premature death
45 (Lelieveld et al., 2015). The Chinese government has attached great importance to improving air
46 quality and issued the “Air Pollution Prevention and Control Action Plan” in September 2013,
47 clearly requiring the concentrations levels of fine particulate matter in a few key regions,
48 including the Pearl River Delta (PRD), to drop by 2017 from 15 to 25% of their values in 2012.
49 The Pearl River Delta is one of the fastest-growing regions in China and the largest urban
50 agglomeration in the world; it includes the cities of Guangzhou, Shenzhen, Zhuhai, Dongguan,
51 Foshan, Huizhou, Zhongshan, Zhaoqing and Jiangmen, and contains more than 58 million people.
52 The PM_{2.5} concentration in this region reached a high level of 58 µg/m³ in 2007 (Nanfang Daily,
53 2016); however, the air quality has significantly improved due to the implementation of strict air
54 pollution control measures, which occurred here earlier than in other regions in China. The annual
55 average concentration of PM_{2.5} in the PRD dropped to 34 µg/m³ in 2015 (Ministry of
56 Environmental Protection, 2016).

57 In recent years, the receptor model method (commonly, positive matrix factorization) in the
58 PRD was applied to perform the source apportionment of PM_{2.5}, which was carried out in several
59 major cities, including Guangzhou (Gao et al., 2013; Liu et al., 2014; Wang et al., 2016),
60 Shenzhen (Huang et al., 2014b), Dongguan (Wang et al., 2015; Zou et al., 2017) and Foshan (Tan
61 et al., 2016). However, the above source apportionment studies only focused on part of PM_{2.5} (e.g.,
62 organic matter) or single city in PRD (e.g., Shenzhen and Dongguan), lacking the extensive
63 representation of the PRD region in terms of simultaneous sampling in multiple cities. Since the
64 lifetime of PM_{2.5} in the surface layer of the atmosphere is days to weeks and the cities in PRD are
65 closely linked, the transport of PM_{2.5} between cities should be specifically noteworthy (Hagler et
66 al., 2006). On the other hand, although the positive matrix factorization (PMF) model has been
67 successfully applied to source apportionment in the PRD, the apportionment with PMF has high
68 rotational ambiguity and can output non-meaningful or mixed factors. Under such conditions, the
69 multilinear engine (ME-2) model can guide the rotation toward a more objective optimal solution
70 by utilizing a priori information (i.e., predetermined factor profiles). In recent years, ME-2,
71 initiated and controlled via the Source Finder (SoFi) written by the Paul Scherrer Institute, was
72 successfully developed to apportion the sources of organic aerosols (Canonaco et al., 2013). The
73 novel ME-2 model has become a widely used and successful source analysis technique (e.g.
74 Crippa et al., 2014; Fröhlich et al., 2015; Visser et al., 2015; Elser et al., 2016; Reyes-Villegas et
75 al., 2016). The key challenges in running ME-2 are the construction of the appropriate constraint
76 source profiles and the determination of factor numbers, and PMF could serve as the first step
77 when using ME-2 for the determination of the priori information needed.

78 Accurately understanding the regional characteristics of PM_{2.5} sources in the PRD can
79 certainly guide the regional joint prevention and control of PM_{2.5} in this region and provide useful
80 references for future air pollution control strategies in China. Thus, in this study, the PM_{2.5} mass
81 and chemical compositions were measured during four seasons in 2015 at six sites in the PRD,
82 which basically represent the pollution level of the PRD on a regional scale rather than on a city

83 scale. For the first time, the novel ME-2 model via the SoFi was applied to a comprehensive
 84 chemical dataset (including EC, OM, inorganic ions and metal elements) to identify the sources of
 85 bulk PM_{2.5} in the regional scale of PRD; then, the spatial locations of the sources were
 86 systematically explored using the analysis of weather conditions.

87 2 Experimental methodology

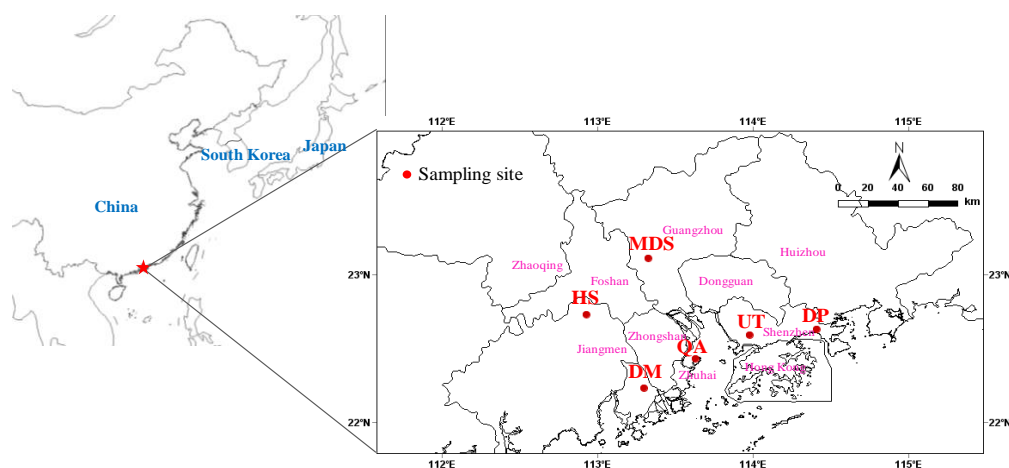
88 2.1 Sampling and chemical analysis

89 The PRD is located in south central Guangdong Province. Based on the layout of the cities in
 90 the PRD, six sampling sites were selected to represent urban, suburban, and background sites.
 91 Detailed descriptions of these sampling sites are listed in Table 1, and their locations are shown on
 92 the regional map in Fig. 1.

93 **Table 1.** Description of the sampling sites in the PRD.

Site	Site code	Coordinates	Site description
Doumen	DM	Lat: N 22.23 Lon: E 113.30	Suburban Contains industrial areas
Qi-Ao island	QA	Lat: N 22.43 Lon: E 113.63	Background An area for eco-tourism
Heshan	HS	Lat: N 22.73 Lon: E 112.93	Suburban Contains industrial areas and farmlands
Modiesha	MDS	Lat: N 23.11 Lon: E 113.33	Urban Contains dense urban traffic
University Town	UT	Lat: N 22.59 Lon: E 113.98	Urban Contains urban traffic
Dapeng	DP	Lat: N 22.63 Lon: E 114.41	Background An area for eco-tourism

94



95

96 **Fig. 1.** Spatial distribution of the sampling sites in the PRD.

97 Samples were collected every other day during a one-month long period for each season in
 98 2015, and Table 2 contains the detailed sampling information to refer to. Each sampling period
 99 lasted for 24 h at each site. The sampling sites of University Town (UT) and Dapeng (DP) used
 100 Thermo 2300 PM_{2.5} samplers (Thermo Fisher Scientific Inc., Waltham, Massachusetts, USA, with

101 a flowrate of 16.7 L/min for two channels and a flowrate of 10.0 L/min for the other two channels),
 102 while those in Modiesha (MDS), Heshan (HS), Qi-Ao Island (QA) and Doumen (DM) used
 103 TH-16A PM_{2.5} samplers (Tianhong Corp., Wu Han, China, with a flow rate of 16.7 L/min for four
 104 channels). Prior to the sampling campaigns, the six samplers used sampled in parallel three times,
 105 and each time lasted for 12 h. The standard deviation of the PM_{2.5} mass concentrations obtained
 106 by the six samplers in each parallel sampling was within 5%. The all sample boxes were then
 107 sealed by Parafilm, stored in an ice-packed cooler during transportation, and stored under
 108 freezing temperatures before analysis. A total of 362 valid samples (15-16 samples at each
 109 site for each season) were collected in this study. In addition, to track the possible
 110 contamination caused by the sampling treatment, a field blank sample was collected at each
 111 site for each season. The PM_{2.5} mass can be obtained based on the difference in the weight of the
 112 Teflon filter before and after sampling in a cleanroom at conditions of 20°C and 50% relative
 113 humidity, according to the Quality Assurance and Quality Control procedures of the National
 114 Environmental Protection Standard (NEPS, MEE, 2013b). The Teflon filters were analyzed for
 115 their major ion contents (SO₄²⁻, NO₃⁻, NH₄⁺ and Cl⁻) via an ion chromatography system
 116 (ICS-2500, Dionex; Sunnyvale, California, USA), following the guidelines of NEPS (MEE, 2016a,
 117 b). The metal element contents (23 species) were analyzed via an inductively coupled plasma
 118 mass spectrometer (ICP-MS, auroraM90; Bruker, Germany), also following the guidelines of
 119 NEPS (MEE, 2013a). The Quartz filters were analyzed for organic carbon (OC) and elemental
 120 carbon (EC) contents using an OC/EC analyzer (2001A, Desert Research Institute, Reno, Nevada,
 121 USA), following the IMPROVE protocol (Chow et al., 1993). The overall organic mass (OM) was
 122 estimated as 1.8×OC. In previous aerosol mass spectrometer (AMS) measurement for PM₁, the
 123 OM/OC ratio was measured to be 1.6 for urban atmosphere (He et al., 2011) and 1.8 for rural
 124 atmosphere (Huang et al., 2011). We adopted a uniform OM/OC ratio of 1.8 in this study
 125 because it is assumed that the mass difference between PM₁ and PM_{2.5} may mostly contain
 126 aged regional aerosol with higher OM/OC.

127 2.2 Meteorological conditions and weather classification

128 The meteorological conditions during the observation period, shown in Table 2, indicated
 129 that the PRD region experienced a hot and humid summer and a cool and dry winter, while spring
 130 and fall were two transition seasons. Furthermore, the back trajectories of the air masses obtained
 131 using the NOAA HYSPLIT model (Fig. S1) revealed that the air masses originated from the
 132 northern inland in winter, from the northern inland and the South China Sea in spring, from the
 133 South China Sea in summer, and from the northeast coast and the northern inland in fall.

134 **Table 2.** General meteorological conditions during the observation period in the PRD.

	Mean (°C)	Temp. (°C)	Rainfall (mm)	Mean RH (%)	Mean wind speed (m/s)	Predominant wind direction
Winter (Jan.10-Feb.9)	17		35	63%	2.1	ENE
Spring (Apr.2-Apr.30)	23		61	72%	1.8	SSW
Summer (Jul.1-Jul.29)	29		244	74%	2.1	SW

135 Changes in meteorological conditions with the seasons have significant influences on the air
 136 quality in the PRD (Hagler et al., 2006). The same type of weather is often repeated. Physick et al.
 137 (2001) classified the weather over the region surrounding Hong Kong into seven categories based
 138 on surface pressure patterns, i.e., as northerly (winter monsoon), northeasterly (winter monsoon),
 139 easterly or southeasterly, trough, southerly or southwesterly (summer monsoon), cyclonic 1 and
 140 cyclonic 2 weather types. The PRD region, including Hong Kong, has nearly the similar weather
 141 patterns and similar meteorological conditions. In this study, the daily weather types during the
 142 observation period (excluding rainy days) were also classified into seven categories based on
 143 surface pressure patterns. However, according to the surface horizontal wind vectors, the PRD was
 144 mostly impacted by two types of airflow, i.e., southerly flow and northerly flow. Southerly flow,
 145 including the southeasterly and southerly or southwesterly (summer monsoon) weather types, was
 146 relatively clean and originated from the ocean (e.g., Fig. S2 and Fig. S4). Northerly flow,
 147 including the northerly (winter monsoon) and northeasterly (winter monsoon) weather types, was
 148 relatively polluted and originated from the north mainland (e.g., Fig. S3 and Fig. S5). Southerly
 149 flow and northerly flow appeared with the highest frequency in the PRD (i.e., above 80%),
 150 followed by cyclone (10%), easterly (2%) and trough (2%). In this study, southerly flow days
 151 ($PM_{2.5} \leq 17 \mu\text{g}/\text{m}^3$, see Table 3) were selected to better reflect the local source regions in the PRD,
 152 and northerly flow days ($PM_{2.5} \geq 75 \mu\text{g}/\text{m}^3$, see Table 3) were selected to better understand the
 153 pollution accumulation process and regional transport characteristics of pollutants in the PRD. The
 154 sampling days for southerly flow and northerly flow are listed in Table 3.

155 **Table 3.** Sampling days categorized as southerly flow and northerly flow days.

Southerly flow	Wind speed (m/s)	$PM_{2.5}$ ($\mu\text{g}/\text{m}^3$)	Northerly flow	Wind speed (m/s)	$PM_{2.5}$ ($\mu\text{g}/\text{m}^3$)
2015.07.01	2.6	16	2015.01.18	2.3	78
2015.07.03	3.6	17	2015.01.20	1.5	82
2015.07.15	1.9	17	2015.02.03	2	75
2015.07.23	2.6	12	2015.02.07	1.7	101
2015.07.25	2	13	2015.02.09	2.2	75
2015.07.29	1.3	12			

156

157 2.3 Input data matrices for source apportionment modeling

158 PMF is a multivariate factor analysis tool widely used for aerosol source apportionment. The
 159 PMF algorithm groups the measured matrix \mathbf{X} (Eq. (1)) into two non-negative constant matrices \mathbf{G}
 160 (factor time series) and \mathbf{F} (factor profiles), and \mathbf{E} denotes the model residuals (Paatero and Tapper,
 161 1994). The entries in \mathbf{G} and \mathbf{F} are fitted using a least-squares algorithm that iteratively minimizes
 162 the object function Q in Eq. (2), where e_{ij} are the elements of the residual matrix \mathbf{E} , and u_{ij} are

163 the errors/uncertainties of the measured species x_{ij} .

$$164 \quad \mathbf{X} = \mathbf{G} \cdot \mathbf{F} + \mathbf{E} \quad (1)$$

$$165 \quad Q = \sum_{i=1}^n \sum_{j=1}^m (e_{ij}/u_{ij})^2 \quad (2)$$

166 The multilinear engine (ME-2) was later developed by Paatero (1999) based on the PMF
 167 algorithm. In contrast to an unconstrained PMF analysis, ME-2 can utilize the constraints (i.e.,

168 predetermined factor profiles) provided by the user to enhance the control of rotation for a more
169 objective solution. One or more factor profiles can be expediently input into ME-2, and the output
170 profiles are allowed to vary from the input profiles to some extent. When using ME-2 modeling,
171 the “mixed factors” can usually be better resolved.

172 In this study, both PMF and ME-2 models were run for the datasets observed in the PRD. We
173 first need to determine the species input into the models. Species that may lead to high species
174 residuals or lower R² values between measured and model-predicted or non-meaning factors were
175 not included, such as those that fulfilled the following criteria: (1) species that were below
176 detection in more than 40% of samples; (2) species that yielded R² values of less than 0.4 in
177 inter-species correlation analysis; and (3) species that had little implication for pollution sources
178 and lower concentrations. Therefore, 18 species were input into the models; these species
179 accounted for 99.6% of the total measured species and included OM, EC, SO₄²⁻, NO₃⁻, NH₄⁺, Cl⁻,
180 K, Ca, Na, Mg, Al, Zn, Fe, Cd, V, Ni, Ti and Pb.

181 The application of PMF or ME-2 also depends on the estimated realistic uncertainty (u_{ij}) of
182 the individual data point of an input matrix, which determines the Q value in Eq. (2). Therefore,
183 the estimation of uncertainty is an important component of the application of these models. There
184 are many sources of uncertainty, including sampling, handling, transport, storage, preparation, and
185 testing (Leiva et al., 2012). In this study, the sources of uncertainty that contributed little to the
186 total uncertainty could be neglected, such as replacing filters, sample transport and sample storage
187 under the strict Quality Assurance and Quality Control. Therefore, we first considered the
188 uncertainties introduced by sampling and analysis processes, such as sampling volume,
189 repeatability analysis and ion extraction. The species uncertainties u_{ij} are estimated using Eq. (3),

190 where \bar{u}_c is the error fraction of the species, which is estimated using the relative combined error
191 formula Eq. (4) (BIPM et al., 2008).

$$192 \quad u_{ij} = \bar{u}_c \times x_{ij} \quad (3)$$

$$193 \quad \bar{u}_c = \sqrt{\bar{u}_f^2 + \bar{u}_r^2 + \bar{u}_e^2} \quad (4)$$

194 where \bar{u}_f is the relative error of the sampling volume; \bar{u}_r is the relative error of the repeatability
195 analysis of the standard species; and \bar{u}_e is the relative error of the ion extraction of multiple
196 samples. When the concentration of the species is below the detection limit (DL), the
197 concentration values were replaced by 1/2 of DL, and the corresponding uncertainties were set at
198 5/6 of DL. Missing values were replaced by the geometric mean of the species with corresponding
199 uncertainties of 4 times their geometric mean (Polissar et al., 1998). The uncertainties of SO₄²⁻,
200 NH₄⁺ and all metal elements, which have scaled residuals larger than ± 3 due to the small
201 analytical uncertainties, need to be increased to reduce their weights in the solution (Norris et al.,
202 2014). In addition, the uncertainties of EC caused by pyrolyzed carbon (PC), the uncertainties of
203 OM, NO₃⁻ and Cl⁻ due to semi-volatility under high ambient temperatures should also be taken

204 into account (Cao et al., 2018). In this study, more reasonable source profiles can be obtained
205 when further increasing the estimated uncertainties (\bar{u}_c) of all species by a factor of 2.

206 **2.4 Constraint setup in ME-2 modeling**

207 In this study, the USEPA PMF v5.0 was applied with the concentration matrix and
208 uncertainties matrix described above to identify the PM_{2.5} sources. After examining a range of
209 factor numbers from 3 to 12, the nine-factor solution output by the PMF base run ($Q_{\text{true}}/Q_{\text{exp}}=2.5$)
210 was found to be the optimal solution, with the scaled residuals approximately symmetrically
211 distributed between -3 and +3 (Fig. S6) and the most interpretable factor profiles (Fig. S7). The
212 model-input total mass of the 18 species and the model-reconstructed total mass of all the factors
213 showed a high correlation ($R^2=0.97$, slope=1.01) (Fig. S8). The factor of biomass burning was not
214 extracted in the eight-factor solution, while the factor of fugitive dust was separated into two
215 non-meaningful factors when more factors were set to run PMF. For the nine-factor solution of
216 secondary sulfate-rich, secondary nitrate-rich, aged sea salt, fugitive dust, biomass burning,
217 vehicle emissions, coal burning, industrial emissions and ship emissions, the source judgment
218 based on tracers for each factor was identical to that of the ME-2 results detailed in Section 3.2.
219 However, in Fig. S7, some factors seemed to be mixed by some unexpected components and were
220 thus overestimated. For example, the secondary sulfate-rich and secondary nitrate-rich factors of
221 PMF had certain species from primary particulates, such as EC, Zn, Al, K and Fe, among which
222 EC had obvious percentage explained variation (EV) values, i.e., the percent of a species
223 apportioned to the factor, of 18.7% and 9.7%, respectively; the EV value of OM in the sea salt
224 factor (which was theoretically negligible) had a high value of 6.4%, and OM accounted for 37%
225 of the total mass of this factor; the EV value of SO_4^{2-} in the fugitive dust factor (which was
226 theoretically negligible) had a high value of 8.6%, and the SO_4^{2-} concentration accounted for 26%
227 of the total mass of this factor.

228 SoFi is a user-friendly interface developed by PSI for initiating and controlling ME-2
229 (Canonaco et al., 2013), and it can conveniently constrain multiple factor profiles. Although
230 USEPA PMF v5.0 can also use some priori information (such as ratio of elements in factor) to
231 control the rotation after the base run, it is not able to use multiple constrained factor profiles to
232 control the rotation (Norris et al., 2014). Therefore, SoFi is a more convenient and powerful tool
233 to establish various constrained factors for source apportionment modeling. Using the same
234 species concentration matrix and uncertainties matrix, we ran the ME-2 model via SoFi for 9–12
235 factors with the four factors constrained as described above, as shown in Table 4. The following
236 considerations were used. Secondary sulfate and secondary nitrate factors should theoretically not
237 contain species from primary particulates, but they may contain secondary organic matter related
238 to the secondary conversion process of SO_2 and NO_x (He et al., 2011; Yuan et al., 2006b; Huang
239 et al., 2014b). Therefore, the contributions of the species from primary particulates were
240 constrained to zero in the input secondary aerosol factors, while others were not constrained. In
241 addition, the factors of sea salt and fugitive dust in primary aerosols could be understood based on
242 the abundance of species in seawater and the upper crust (Mason, 1982; Taylor and McLennan,
243 1995). As seen in Table S1, the abundances of Cl^- , Na^+ , SO_4^{2-} , Mg^{2+} , Ca^{2+} and K^+ in sea salt were
244 relatively high, as were the abundances of Al, Fe, Ca, Na, K, Mg and Ti in fugitive dust. Therefore,
245 these high-abundance species were not constrained in the sea salt and fugitive dust factors, while
246 the other species (with abundances of less than 0.1% in the particulates) were constrained to zero

247 (Table 4). In addition, HNO_3 might react with sea salt to displace Cl^- (Huang et al., 2006); thus,
 248 NO_3^- was also not constrained in the sea salt factor.

249 **Table 4.** The constraints of factor species for ME-2 modeling.

Factors	OM	EC	Cl^-	NO_3^-	SO_4^{2-}	NH_4^+	Ca	Ti	V	Ni	Zn	Cd	Pb	Na	Mg	Al	K	Fe
Secondary sulfate	—	0	0	0	—	—	0	0	0	0	0	0	0	0	0	0	0	0
Secondary nitrate	—	0	0	—	0	—	0	0	0	0	0	0	0	0	0	0	0	0
Sea salt	0	0	—	—	—	0	—	0	0	0	0	0	0	—	—	0	—	0
Fugitive dust	0	0	0	0	0	0	—	—	0	0	0	0	0	—	—	—	—	—

250

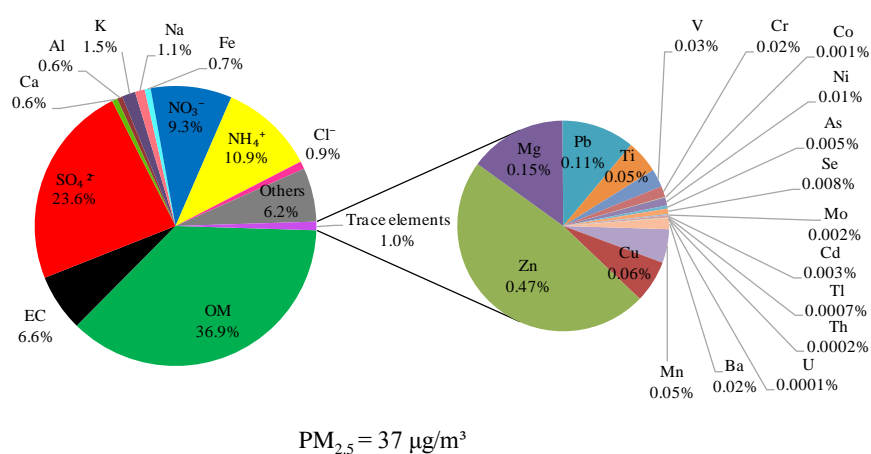
251 3 Results and discussion

252 3.1 Tempo-spatial variations of $\text{PM}_{2.5}$ in the PRD

253 The 4-month average $\text{PM}_{2.5}$ concentration for all six sites in the PRD was $37 \mu\text{g}/\text{m}^3$, which was
 254 slightly higher than the Grade II national standards for air quality (with an annual mean of 35
 255 $\mu\text{g}/\text{m}^3$). The chemical compositions of $\text{PM}_{2.5}$ in the PRD are shown in Fig. 2. OM had the highest
 256 contribution of 36.9%, suggesting severe organic pollution in the PRD. Other important
 257 components included SO_4^{2-} (23.6%), NH_4^+ (10.9%), NO_3^- (9.3%), EC (6.6%) and Cl^- (0.9%).
 258 The major metallic components included K (1.5%), Na (1.1%), Fe (0.7%), Al (0.6%), and Ca
 259 (0.6%), and trace elements accounted for 1.0%. Fig. 3a shows the spatial distribution of the $\text{PM}_{2.5}$
 260 and chemical components between six sites. The $\text{PM}_{2.5}$ pollution level in the PRD was distinctly
 261 higher in the northwestern hinterland (HS and MDS) and lower in the southern coastal areas (DM
 262 and DP). The DP background site had little local emission and was hardly influenced by the
 263 emissions from the PRD under both southerly flow and northerly flow. Thus, its air pollution
 264 reflects the large-scale regional air pollution. The average $\text{PM}_{2.5}$ concentration at DP was as high
 265 as $28 \mu\text{g}/\text{m}^3$, indicating that the PRD had a large amount of air pollution transported from outside
 266 this region. At the background DP site, the fractions of Cl^- and NO_3^- in $\text{PM}_{2.5}$ were the lowest of
 267 the six sites, i.e., 0.3% and 3.9%, respectively, suggesting that they had dominantly local sources
 268 in the PRD. The highest concentration level of $\text{PM}_{2.5}$ was observed at HS (suburban), which was
 269 influenced by the pollution transport of Foshan (industrial city) and Guangzhou (metropolis) under
 270 the northeastern wind, which is the most frequent wind in the PRD. The back trajectories of the air
 271 masses (Fig. S1) show that the northern monsoon prevails in winter and the southern monsoon
 272 prevails in summer in the PRD. Under the winter monsoon, the air masses mostly came from the
 273 inland and carried higher concentrations of air pollutants. However, under the summer monsoon,
 274 the air masses largely originated from the South China Sea and were clean. In addition, the
 275 frequent rainfall and higher planetary boundary layer (PBL) in summer in the PRD also favored
 276 the dispersion and removal of air pollutants (Huang et al., 2014b). Fig. 3b shows that the
 277 normalized seasonal variations of the major components in $\text{PM}_{2.5}$ in the PRD were evidently
 278 higher in winter and lower in summer, which is consistent with the seasonal variations of monsoon
 279 and other meteorological factors as mentioned above.

280 Table 5 summarizes some previous studies that used similar filter-sampling and
 281 analytical methods to allow for a better comparison with this study. In 2002-2003, Hagler et al.
 282 (2006) also conducted observations and analysis of $\text{PM}_{2.5}$ in the PRD and Hong Kong region,
 283 nearly 12 years before this study, as shown in Table 5. Compared with Hagler's results, the $\text{PM}_{2.5}$
 284 concentrations in this study decreased by 42% in Guangzhou (MDS) and 21% in Shenzhen (UT),
 285 especially OC, EC and SO_4^{2-} , which decreased significantly by 20%–47%, indicating that the

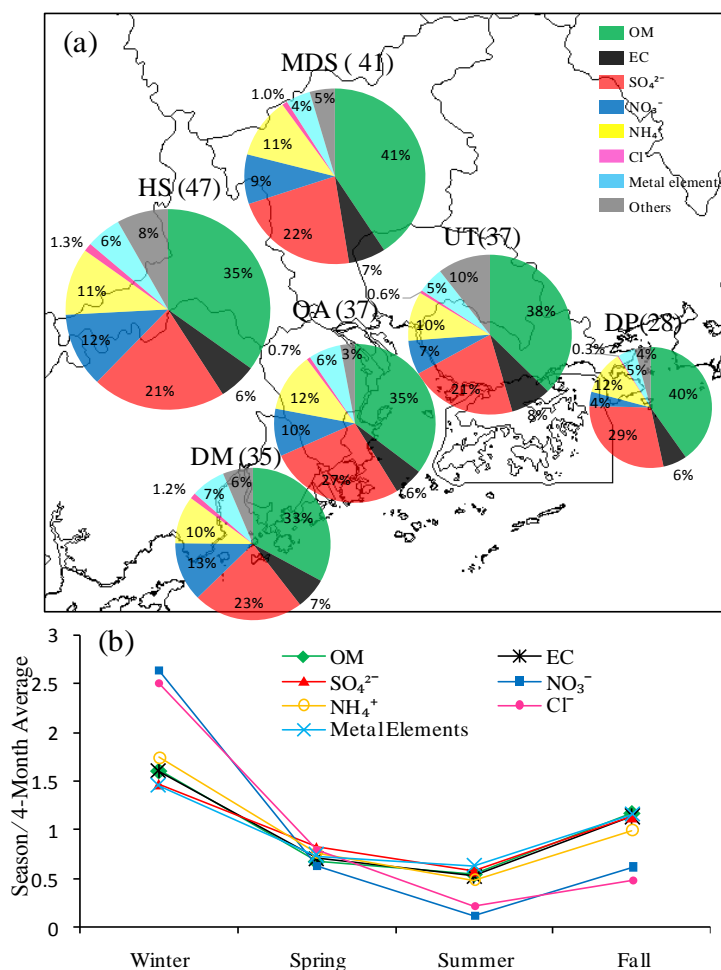
286 measures taken to desulfurize coal-fired power plants, improve the fuel standards of motor
 287 vehicles and phase-out older and more polluting vehicles have played important roles in
 288 improving the air quality in the PRD region (People's Government of Guangdong Province, 2012).
 289 Compared with the PM_{2.5} concentrations reported by other cities in China in recent years, the
 290 PM_{2.5} concentrations in urban Guangzhou and Shenzhen in this study were 39%–63% lower than
 291 those in Beijing (Huang et al., 2017) in northern China, Shanghai (Ming et al., 2017) in eastern
 292 China, and Chengdu (Wang et al., 2018) in western China. However, the PM_{2.5} concentrations in
 293 urban Guangzhou and Shenzhen observed in this study were clearly higher than those in famous
 294 mega-cities in developed countries, such as Paris (Bressi et al., 2013), London (Rodríguez et al.,
 295 2007), and Los Angeles (Hasheminassab et al., 2014), while they were similar to those of Santiago
 296 (Villalobos et al., 2015) and Chuncheon (Cho et al., 2016). It should be highlighted that the higher
 297 concentration of SO₄²⁻ in the urban atmosphere of the PRD is one of the major reasons leading to
 298 the higher degree of PM_{2.5} pollution in the PRD compared to those in developed cities.



299

300

Fig. 2. Chemical compositions of 4-month average PM_{2.5} in the PRD region.



301

302 **Fig. 3.** The spatial distributions (a) and seasonal variations (b) of the PM_{2.5} chemical compositions in the PRD.

303 Sizes of the pie charts indicate the concentrations of PM_{2.5} at the six sites, with the detailed numbers (unit: μg/m³)

304 in brackets.

305

306

Table 5. The comparison of the major chemical compositions of PM_{2.5} in typical cities (unit: μg/m³).

Cities	Periods	PM _{2.5}	OC	EC	SO ₄ ²⁻	NO ₃ ⁻	NH ₄ ⁺	References
Zhuhai (DM)	2015.1–2015.11	35	6.4	2.3	8.1	4.4	3.6	This study
Zhuhai (QA)		37	7.2	2.2	9.9	3.5	4.4	
Jiangmen (HS)		47	9.0	2.8	9.8	5.6	5.0	
Guangzhou (MDS)		41	9.3	2.7	9.2	3.7	4.6	
Shenzhen (UT)		37	7.8	3.0	8.0	2.6	3.7	
Shenzhen (DP)		28	6.2	1.8	8.0	1.1	3.3	
Hong Kong (Urban)	2002.10–2003.6	34.3	6.6	1.9	9.3	1.0	2.5	Hagler et al., 2006
Shenzhen (Urban)		47.1	11.1	3.9	10.0	2.3	3.2	
Guangzhou (Urban)		70.6	17.6	4.4	14.7	4.0	4.5	
Beijing	2014.6–2015.4	99.5	15.5	6.2	14.3	17.9	11.5	Huang et al., 2017
Shanghai	2013.9–2014.8	94.6	9.89	1.63	14.5	18.0	8.13	Ming et al., 2017
Chengdu/Sichuan	2014.10–2015.7	67.0	10.9	3.6	11.2	9.1	7.2	Wang et al., 2018
Paris/France	2009.9–2010.9	14.8	3.0	1.4	2.0	2.9	1.4	Bressi et al., 2013

London/United Kingdom	2003.12–2005.4	31.0	5.6	1.6	2.8	3.5	2.1	Rodríguez et al., 2007
Los Angeles/United States	2002–2013	17.1	2.2	1.3	2.7	4.9	0.1	Hasheminassab et al., 2014
Santiago/Chile	2013.3–2013.10	40	12.1	4.3	1.9	7.1	3.3	Villalobos et al., 2015
Chuncheon/Korea	2013.1–214.12	34.6	9.0	1.6	3.9	2.8	2.0	Cho et al., 2016

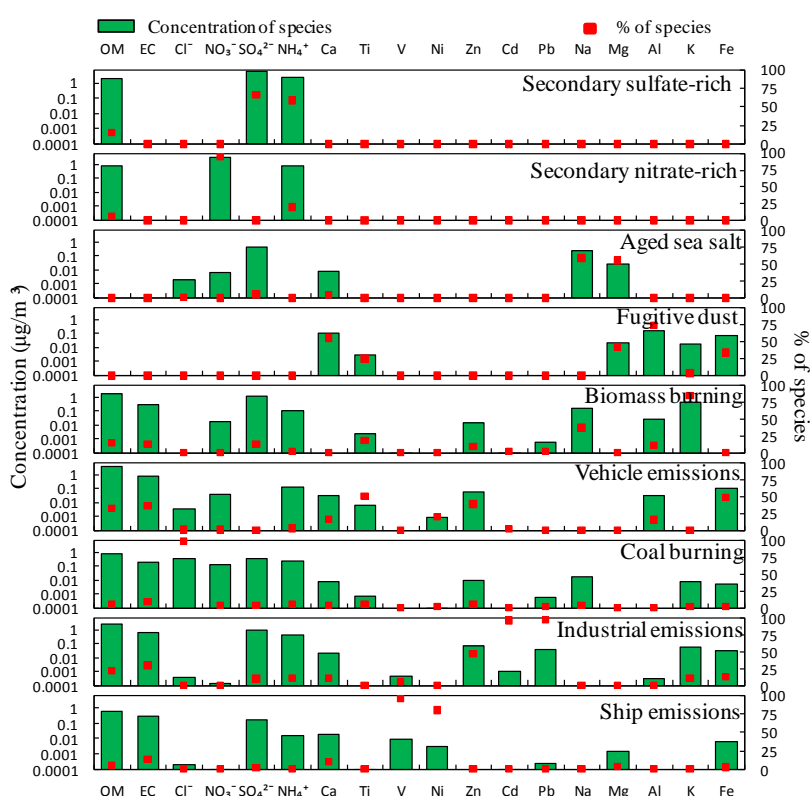
307

308 3.2 Source apportionment of PM_{2.5} using ME-2

309 The solutions of 9–12 factors of the ME-2 were modeled with the four factors constrained in
310 Table 4, using the SoFi tool, an implementation of ME-2 (Canonaco et al., 2013). Again, the
311 nine-factor solution provided the most reasonable source profiles, since non-interpretable factors
312 were produced (e.g., a Ti-high factor) when more factors were set to run ME-2. Based on the EV
313 and the contributed concentrations of species in each factor shown in Fig. 4, the sources of PM_{2.5}
314 can be judged as follows: (1) the first factor was explained as secondary sulfate-rich, which had
315 large EV values of SO₄²⁻ and NH₄⁺. (2) The second factor was explained as secondary nitrate-rich,
316 which had significant EV values of NO₃⁻ and NH₄⁺. (3) The third factor was related to sea salt
317 due to the large EV values and concentrations of Na and Mg. However, the low Cl⁻ concentration
318 and high SO₄²⁻ concentration implied that SO₄²⁻ replaced Cl⁻ during the sea salt aging process.
319 Therefore, this factor was identified as aged sea salt (Yuan et al., 2006a). (4) The fourth factor was
320 identified as fugitive dust due to its significant EV values of Al, Ca, Mg and Fe. In this study, the
321 undetermined mass of O and Si in this factor was compensated using the elemental abundance in
322 dust particles in Table S1 (Taylor and McLennan, 1995). (5) The fifth factor was identified as
323 biomass burning due to its significant characteristic value of K (Yamasoe et al., 2000). (6) The
324 sixth factor had high concentrations and large EV values of OM and EC, as well as a certain range
325 of EV values of Fe and Zn, which were related to tires and the brake wear of motor vehicles (Yuan
326 et al., 2006a; He et al., 2011). Therefore, this factor was identified as vehicle emissions. (7) The
327 seventh factor had a high EV value of Cl⁻ and certain concentrations of OM, EC, SO₄²⁻ and NO₃⁻,
328 implying a combustion source. This factor was identified as coal burning, which was a major
329 source of Cl⁻ in the PRD (Wang et al., 2015). (8) The eighth factor had large EV values of Zn, Cd
330 and Pb, and certain concentrations of OM and EC. Zn, Cd and Pb had high enrichment factors
331 (Table S2) of 821, 4121 and 663, respectively, and were thus considered to be related to industrial
332 emissions (Wang et al., 2015). (9) The last factor had large EV values of V and Ni. V and Ni were
333 predominantly derived from heavy oil combustion, and they had high enrichment factors (Table
334 S2) of 64 and 89, respectively. Heavy oil was related to ship emissions in the PRD (Chow et al.,
335 2002; Huang et al., 2014b). Although these nine factors of the ME-2 modeling generally showed
336 high correlations (R²=0.81–0.97) with the corresponding factors of the PMF modeling in terms of
337 time series, it is easy to see that the ME-2 modeling provided a better Q_{true}/Q_{exp} ratio (1.2) than
338 that of the PMF modeling (Q_{true}/Q_{exp}=2.5), indicating that the species residuals were decreased in
339 the ME-2 modeling, and the EV values of tracers (e.g., SO₄²⁻, NO₃⁻, OM, EC, Cl⁻, V, Ni, Pb and
340 Cd) were assigned to factors more intensively. Therefore, it is concluded that the source
341 apportionment results of the ME-2 modeling were more environmentally meaningful and
342 statistically better than those of the PMF modeling.

343 In this study, secondary organic aerosol (SOA) did not appear as a single factor, even if we
344 run the ME-2 with ten or more factors. SOA can usually be described by low-volatile oxygenated
345 organic aerosol (LV-OOA) and semi-volatile oxygenated organic aerosol (SV-OOA), based on the
346 volatility and oxidation state of organics (Jimenez et al., 2009). In previous studies (e.g., He et al.,

347 2011; Lanz et al., 2007; Ulbrich et al., 2009), the time series of LV-OOA and SV-OOA were
 348 highly correlated with those of sulfate and nitrate, respectively, implying that LV-OOA and
 349 sulfate (or SV-OOA and nitrate) cannot be separated easily in cluster analysis, especially when
 350 there is no effective tracer of SOA. In this study, the high OM concentration in the secondary
 351 sulfate-rich factor was considered to represent LV-OOA, while the high OM concentration in the
 352 secondary nitrate-rich factor was considered to represent SV-OOA (Yuan et al., 2006b; He et al.,
 353 2011). Therefore, it should be acknowledged that mixed secondary factors cannot be solved even
 354 using ME-2. However, the contribution time-series of LV-OOA (or SV-OOA) can be extracted
 355 based on the contribution time-series of the secondary sulfate-rich factor (or the secondary
 356 nitrate-rich factor) and the mass percentage of OM in this factor, leaving the remaining mass as
 357 the “pure” secondary sulfate (or secondary nitrate). Therefore, a new SOA factor can be
 358 reasonably estimated by LV-OOA+SV-OOA.



359

360

Fig. 4. The factor profiles and explained variations of the ME-2 modeling.

361

362

363

364

365

366

367

Fig. 5 shows the 4-month average contributions of the PM_{2.5} sources in the PRD in 2015 based on the source apportionment of ME-2. The total secondary aerosols accounted for 39% of PM_{2.5} in the PRD, which were secondary sulfate (21%), secondary nitrate (11%) and SOA (7%). However, the identified primary particulates contributed 54% of PM_{2.5}, which comprised vehicle emissions (14%), industrial emissions (13%), biomass burning (11%), coal burning (6%), fugitive dust (5%), ship emissions (3%) and aged sea salt (2%). The unidentified sources, including both the residual from ME-2 and the unmeasured species, accounted for 7%.

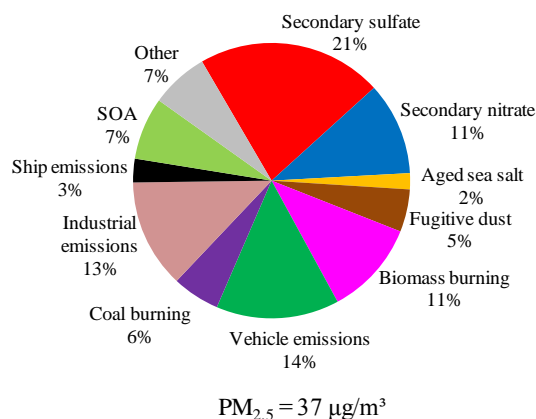


Fig. 5. The 4-month average contributions of $PM_{2.5}$ sources in the PRD.

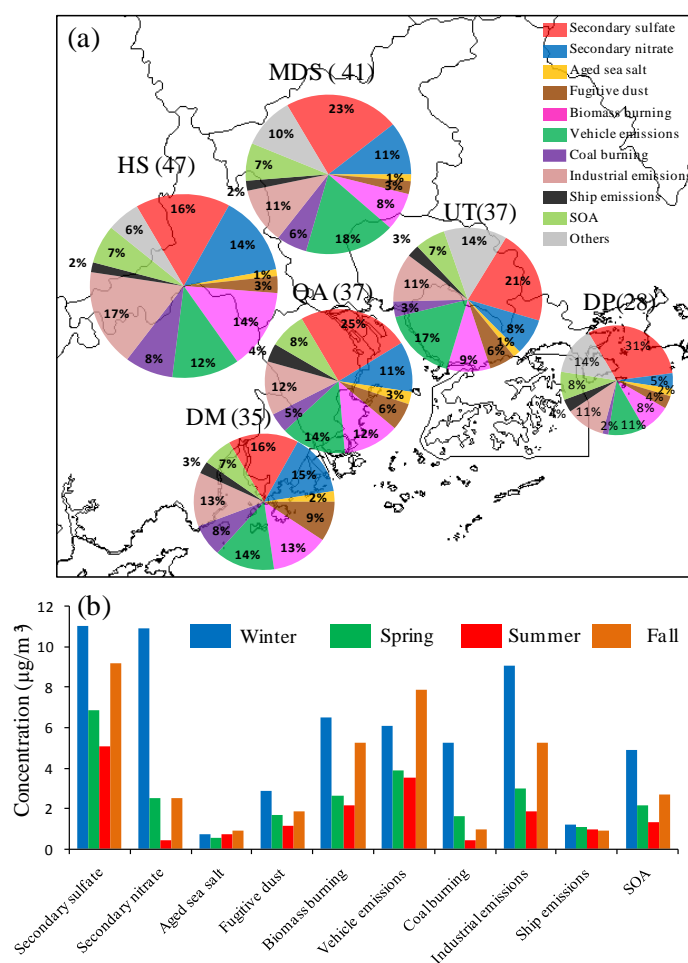
3.3 Tempo-spatial variations of sources in the PRD

The spatial distributions of the $PM_{2.5}$ sources between six sites are shown in Fig. 6a. Secondary sulfate represented the largest fraction (31%) of $PM_{2.5}$ at DP, indicating that it was a major air pollutant in the air mass transported to the PRD. Vehicle emissions also contributed relatively highly to urban sites (18% in MDS and 17% in UT). Industrial emissions, biomass burning, secondary nitrate, and coal burning contributed larger fractions of $PM_{2.5}$ at HS, which could be attributed to both strong local sources (e.g., the surrounding township factories and farmlands) and regional transport from upwind cities at this site. Fugitive dust, which is primarily related to construction activities, was relatively high at DM (9%). The contributions of ship emissions and aged sea salt were the highest at QA due to the site being located on Qi-Ao Island in the Pearl River Estuary, which records the greatest impact from the sea. SOA contributed similar amounts (7%–8%) at all sites. It should be noted that, although QA was a background site without local anthropogenic sources, its $PM_{2.5}$ level was moderate in the PRD, indicating that QA was impacted by severe regional transport from the surrounding cities.

Fig. 6b shows the seasonal variations of the major sources of $PM_{2.5}$ in the PRD. The contributions of most sources were higher in winter and lower in summer, e.g., secondary sulfate, secondary nitrate, fugitive dust, biomass burning, vehicle emissions, coal burning, industrial emissions and SOA; these sources were greatly influenced by the seasonal variations of monsoon, rainfall and PBL, as discussed in Section 3.1. For example, although secondary sulfate was proven to be a typical regional pollutant in the PRD (Huang et al., 2014b; Zou et al., 2017), the more polluted continental air mass in the winter monsoon made its concentrations in winter much higher than in summer. The semi-volatile secondary ammonium nitrate was also significantly affected by seasonal ambient temperatures. In contrast, the average contributions of aged sea salt and ship emissions for the whole region displayed little seasonal variations, consistent with that the emissions were from local surrounding sea areas.

Previous studies of the source apportionment of bulk $PM_{2.5}$ in the PRD have mainly focused on Guangzhou, Dongguan and Shenzhen, as seen in Table 6. It can be seen that in those studies, $PM_{2.5}$ was apportioned to 6–9 sources and that secondary sulfate was the prominent source, although the results of different studies exhibited certain differences due to the use of different models or data inputs. Compared with the study of Huang et al. (2014b) in Shenzhen in 2009, the contributions of secondary sulfate and vehicle emissions in Shenzhen in this study were obviously lower due to power plant desulfurization and motor vehicle oil upgrades in recent years (People's

402 Government of Shenzhen Municipality, 2013). Compared with previous studies in Guangzhou,
 403 this study attained more PM_{2.5} sources, which can more clearly describe the source structure of
 404 PM_{2.5} in this region, especially industrial emissions (11%). The PRD region has experienced a
 405 high degree of industrialization; thus, industrial sources should be a major source, contributing
 406 8.1% of PM_{2.5} reported by the Guangzhou Environmental Protection Bureau (2017), similar to our
 407 results. Tao et al. (2017) apportioned PM_{2.5} to 6 sources using PMF in Guangzhou, including some
 408 mixed sources. For example, ship emissions in Tao's study may not actually represent a primary
 409 source due to the significant existence of some secondary inorganics and sea salt in the source
 410 profile; thus, they obtained a significantly higher contribution (17%) than that in our study. Ship
 411 emissions were unidentified in Huang's study (2014a) in Guangzhou.



412
 413 **Fig. 6.** The spatial distributions (a) and seasonal variations (b) of PM_{2.5} sources in the PRD. Sizes of the pie charts
 414 indicate the concentrations of PM_{2.5} at the six sites, with the detailed numbers (unit: µg/m³) in brackets.

415
 416

Table 6. Comparison of the results of source apportionment of PM_{2.5} in the PRD.

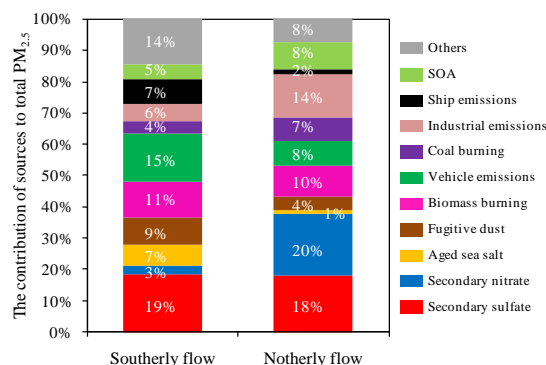
Cities	Periods	Model	Results	References
Shenzhen	2015.1—2015.11 (Four seasons)	ME-2	Secondary sulfate (21%), secondary nitrate (8%) and SOA (7%), vehicle emissions (17%), industrial emissions (11%), biomass burning (9%), coal burning (3%), fugitive dust (6%), ship emissions (3%) and aged sea salt (1%).	This study
Shenzhen	2009.1—2009.12 (Four seasons)	PMF	Secondary sulfate (30.0%), vehicular emission (26.9%), biomass burning (9.8%), secondary nitrate (9.3%), high chloride (3.8%), heavy oil combustion (3.6%),	Huang et al. (2014b)

			sea salt (2.6%), dust (2.5%), metallurgical industry (2.1%).	
Guangzhou	2015.1—2015.11 (Four seasons)	ME-2	Secondary sulfate (23%), secondary nitrate (11%), SOA (7%), vehicle emissions (18%), industrial emissions (11%), biomass burning (8%), coal burning (6%), fugitive dust (3%), ship emissions (2%) and aged sea salt (1%).	This study
Guangzhou	2014.1—2014.12 (Four seasons)	PMF	Secondary sulfate and biomass burning (38%), ship emissions (17%), coal combustion (15%), traffic emissions (10%), secondary nitrate and chloride (12%), soil dust (7%).	Tao et al. (2017)
Guangzhou	2015.1—2015.2 (Winter)	ME-2	Secondary sulfate (20%), secondary nitrate (16%), SOA (8%), vehicle emissions (11%), industrial emissions (13%), biomass burning (6%), coal burning (9%), fugitive dust (2%), ship emissions (1%) and aged sea salt (1%).	This study
Guangzhou	2013.1 (Winter)	ME-2	Secondary inorganic-rich (59.0%), secondary organic-rich (18.1%), traffic (8.6%), coal burning (3.4%), biomass burning (6.7%), cooking (0.8%), dust related (3.4%).	Huang et al. (2014a)
Dongguan	2013.12—2014.11 (Four seasons)	PMF	Secondary sulfate (20%), secondary nitrate (8%), SOA (10%), vehicle emissions (21%), industrial emissions (7%), biomass burning (11%), coal burning (5%), fugitive dust (8%), ship emissions (6%).	Zou et al. (2017)
Dongguan	2010.2—2012.12 (Four seasons)	PMF	Secondary sulfate (27%), secondary nitrate (19%), industrial emission (15%), biomass burning (9%) and coal combustion (9%); ship emissions/sea salt, vehicle exhaust, plastic burning and dust no more than 7%.	Wang et al. (2015)

417

418 3.4 Identification of high-emission areas in the PRD in typical meteorological conditions

419 Fig. 7 shows the contributions of PM_{2.5} sources under southerly flow and northerly flow
 420 conditions in the PRD, based on the classification of weather types in Section 2.2. Southerly flow
 421 primarily originated from the South China Sea and carried clean ocean air masses to the PRD with
 422 overall PM_{2.5} values of 15 µg/m³. As shown in Fig. 7, secondary sulfate (19%), vehicle emissions
 423 (15%) and biomass burning (11%) had higher contributions under southerly flow. In contrast, in
 424 northerly flow, the level of PM_{2.5} (82 µg/m³) was 4.5 times higher than that of southerly flow due
 425 to the transport of polluted air masses southward from the north mainland. Under northerly flow,
 426 secondary sulfate (18%) and biomass burning (10%) were still the major sources, but secondary
 427 nitrate became the dominant source of PM_{2.5}, accounting for 20% of PM_{2.5}. In addition, industrial
 428 emissions also exhibited a relatively high contribution (14%).



429

430 **Fig. 7.** The contributions of PM_{2.5} sources under southerly flow and northerly flow conditions in the PRD.

431 The spatial distributions of the PM_{2.5} sources under southerly flow and northerly flow are
 432 shown in Fig. 8. The high-emission areas for different sources identified by the discussion below
 433 are marked on the map in Fig. 9. The average concentration levels of aged sea salt were similar in

434 the summer southerly flow and the winter northerly flow, reflecting local release of sea salt. The
435 spatial distribution of aged sea salt among the different sites was a complex result of the site
436 locations relative to the sea and meteorological conditions, e.g., wind and tide. A relatively high
437 level of aged sea salt was observed at the Qi-Ao Island (QA), especially in the northerly flow,
438 which can be attributed to that the QA site was surrounded by the sea and had lower wind speeds
439 in the northerly flow (in Table 3).

440 The influences of ship emissions exhibited large differences between six sites, showing
441 significant local characteristics. In addition, the ship emissions have similar average
442 concentrations in the summer southerly flow and winter northerly flow, also reflecting the
443 emissions of local ports in the PRD region. The concentrations of ship emissions were the highest
444 at DP under southerly flow, mainly due to the impact of vessels in the upwind Yiantian Port, while
445 they were the highest at QA under northerly flow, primarily due to the effects of the upwind
446 Nansha Port, as shown in Fig. 9. Yantian Port and Nansha Port are among the ten largest ports in
447 the world (Hong Kong Marine Department, 2012).

448 The contributions of fugitive dust also exhibited significant differences between six sites,
449 which are consistent with local construction activities. DM is located in a newly developed zone
450 that has experienced relatively high levels of fugitive dust during southerly flow and northerly
451 flow due to active construction activities. Sample records indicate that the high value of fugitive
452 dust at UT under southerly flow maybe related to its surrounding short-term road construction
453 project, while the high value at QA under northerly flow maybe related to the reconstruction
454 project of the adjacent Nansha Port (Guangzhou Municipal People's Government, 2015).

455 Motor vehicles are a common source of air pollution in the highly urbanized and
456 industrialized PRD region. The average concentration of vehicle emissions during northerly flow
457 was nearly 3-fold that during southerly flow. Under southerly flow, MDS, HS and UT, which are
458 located in the hinterland of the PRD, had much higher levels of vehicle emissions than the other
459 three sites; in particular, the highest level at the urban MDS site was caused by the high density of
460 motor vehicles in Guangzhou. Under northerly flow, the highest concentration of vehicle
461 emissions was still at the urban MDS site, while QA also recorded the prominent contribution of
462 vehicle emissions, which was probably closely related to the container trucks in the neighboring
463 Nansha Port. It should be noted that the concentration of vehicle emissions at the background DP
464 site exceeded half the regional average value, approaching $4 \mu\text{g}/\text{m}^3$, thus indicating that vehicle
465 emissions had a significant impact on the regional transport of air masses from the north.

466 During southerly air flow, the background DP and QA sites and the urban UT site all
467 recorded similar concentrations of secondary sulfate, suggesting that the secondary sulfate at these
468 sites was dominated by regional transport from the southern ocean with heavy vessel transport and
469 had little to do with the urban emissions at UT. Kuang et al. (2015) also found that ship emissions
470 could be a major source of secondary sulfate in the PRD in summer. HS and MDS had
471 significantly higher concentrations than their upwind site, DM, suggesting that the area between
472 MDS and HS could be a high-SO₂-emission area, which is consistent with the fact that this area is
473 an intensive industrial area. During northerly air flow in winter, HS and DM had lower
474 concentrations than the four upwind sites, i.e., MDS, QA, UT, and especially DP (the background
475 site), indicating that secondary sulfate could mainly be derived from regional transport from
476 outside the PRD in this season. Although the industrial area between HS and MDS could emit
477 significant amounts of SO₂, the lower temperatures and dry air in winter did not appear to favor

478 the quick conversion of SO₂ to secondary sulfate. Since both secondary sulfate and LV-OOA
479 belong to a mixed factor with fixed proportions, the spatial distribution of secondary sulfate also
480 reflects the corresponding characteristics of LV-OOA.

481 The spatial distributions of coal burning were significantly different between the six sites
482 during periods of both south wind and north wind, thus showing conspicuous local characteristics.
483 The contribution of coal burning was higher at MDS under southerly flow and higher at HS under
484 northerly flow. Most of the coals in the PRD were consumed by thermal power plants, but there
485 were no coal-fired power plants near the urban MDS and background DP sites. Therefore, it is
486 speculated that the high-emission areas of coal burning sources mainly exist in the region between
487 HS and MDS, as shown in Fig. 9. The distributions of coal-fired power plants in Guangdong
488 (Wang et al. 2017) reveal that some important coal-fired power plants are distributed in this region.
489 Additionally, DM also exhibited relatively obvious contributions of coal burning during southerly
490 flow and northerly flow, which is also consistent with the distribution of coal-fired power plants in
491 the vicinity.

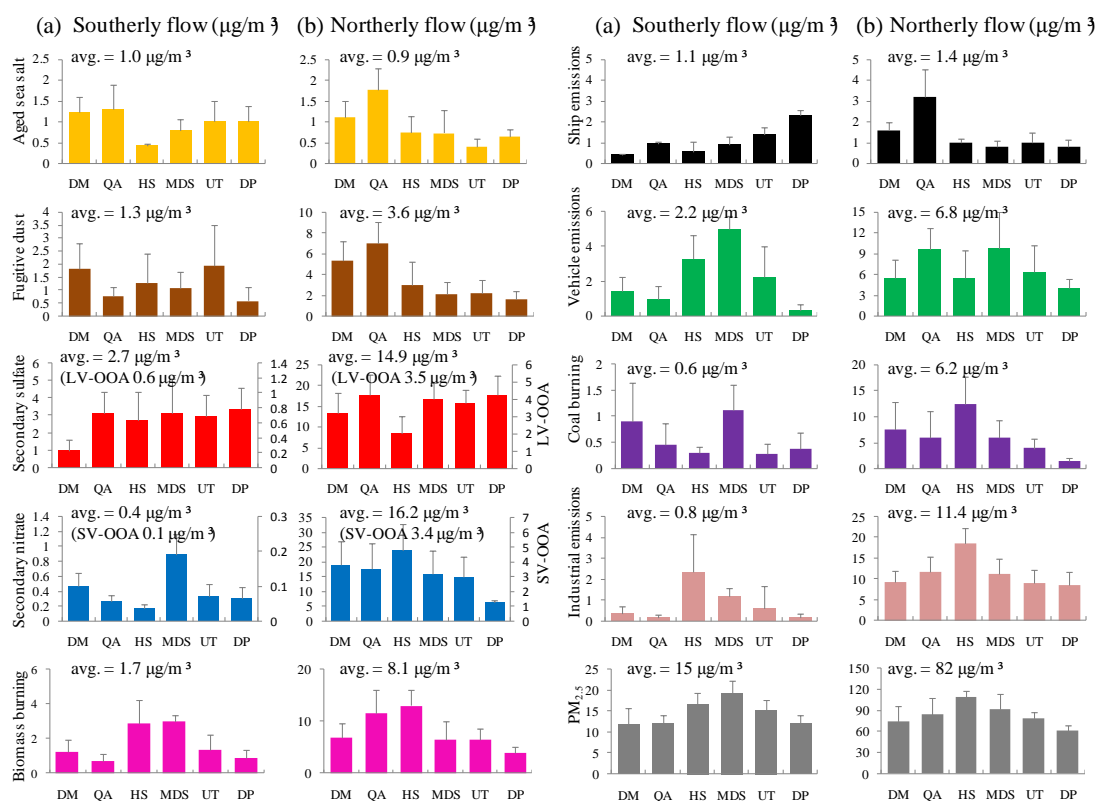
492 The average concentration of secondary nitrate during northerly flow in winter was 40 times
493 greater than that during southerly flow in summer; this occurred not only because of the
494 unfavorable conditions of atmospheric diffusion in winter but also due to the high semi-volatility
495 of ammonium nitrate, which cannot stably exist in fine particles in the PRD during hot summer
496 (Huang et al. 2006). Under southerly flow conditions, the concentrations of secondary nitrate
497 presented prominent differences between six sites, showing local characteristics. Moreover, the
498 relatively low concentrations at the background DP site during northerly flow also indicated that
499 secondary nitrate mainly originated from the interior of the PRD. The spatial distribution
500 characteristics of secondary nitrate were very similar to those of coal burning, with the highest
501 occurring at MDS under southerly flow, the highest occurring at HS under northerly flow and
502 significantly high values occurring at DM under southerly and northerly flow, displaying that the
503 NO_x emissions produced by coal burning maybe the main reason for the high nitrate levels in
504 those areas. Since both secondary nitrate and SV-OOA belong to a mixed factor with fixed
505 proportions, the spatial distribution of secondary nitrate also reflects the corresponding
506 characteristics of SV-OOA.

507 Under southerly flow, the influence of industrial emissions differed vastly between six sites,
508 showing obvious local characteristics. Under northerly flow, the average concentration of
509 industrial emissions reached 14-fold that of southerly flow, and the high contributions at
510 background DP suggested that regional transport probably dominated the industrial sources of fine
511 particulate matter in the PRD in winter. HS had the highest concentration of industrial emissions
512 during southerly flow and northerly flow conditions, which is consistent with the dense factories
513 present in the surrounding area (Hu, 2004; Environmental Protection Agency of Jiangmen City,
514 2017). In addition, the contribution of industrial emissions was relatively high at MDS during
515 southerly flow and relatively high at QA during northerly flow, which supports the inference that a
516 high-emission region of industrial sources was located between MDS and QA, as seen in Fig. 9.

517 The impacts of biomass burning exhibited relatively large differences between six sites
518 during both south and north wind conditions, presenting somewhat local characteristics. Suburban
519 HS site had relatively high biomass burning levels during southerly flow and northerly flow,
520 which should be related to the presence of many farmlands in its vicinity and thus the popular
521 events of open burning and residential burning of biomass wastes. The concentrations of biomass

522 burning were relatively high at the urban MDS site during southerly flow and relatively high at the
 523 background QA site during northerly flow, implying that there was a high-emission area of
 524 biomass burning between MDS and QA, as shown in Fig. 9. Those spatial distribution
 525 characteristics of biomass burning were similar to those of industrial emissions in the PRD,
 526 suggesting that not only the combustion of residential biomass but also the use of industrial
 527 biomass-boilers could make important contributions to $PM_{2.5}$ in the PRD.

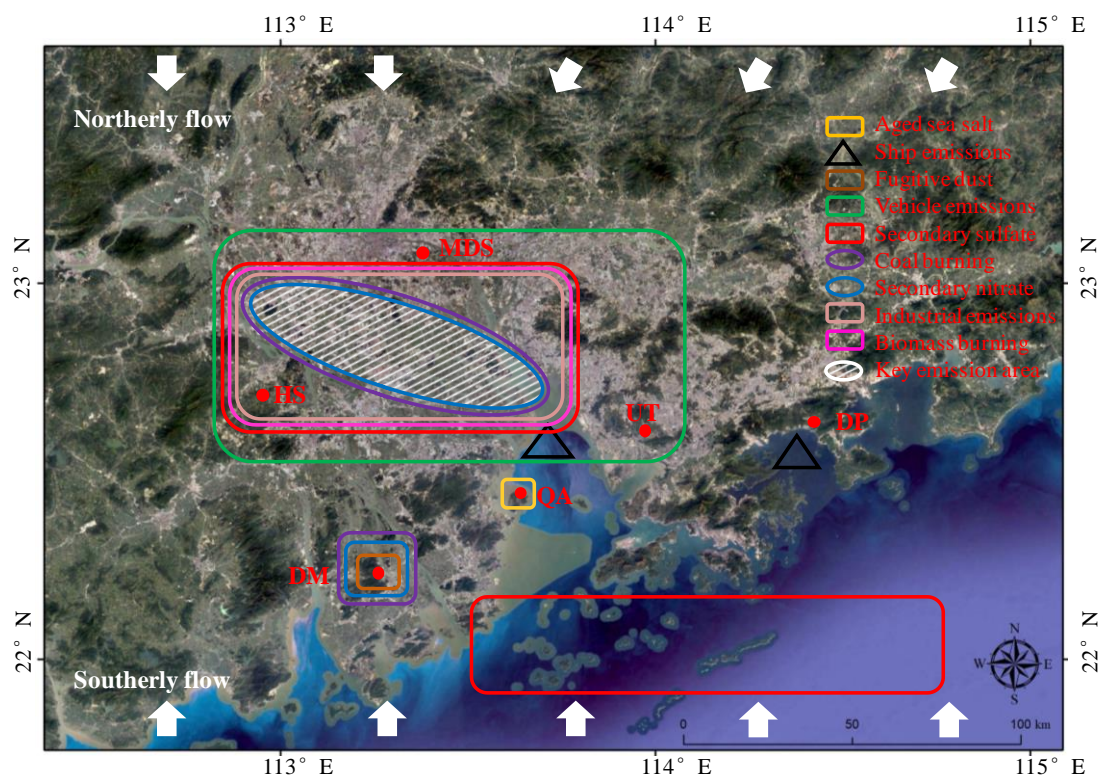
528 As a summary, the central PRD area, i.e., the middle region between MDS, HS and QA (the
 529 shaded region in Fig. 9), represents the most important pollutant emissions area in the PRD; these
 530 emissions include SO_2 , NO_x , coal burning, biomass burning, industrial emissions and vehicle
 531 emissions, thus leading to high pollution levels in the PRD. Therefore, this area is a key area for
 532 pollution control in the PRD. Primary fine particulate matter and SO_2 from ship emissions had
 533 significant impacts on $PM_{2.5}$ in the southern coastal area of the PRD during summer southerly
 534 flow, and special attention must be paid to them.



535

536 **Fig. 8.** The average contributions of $PM_{2.5}$ sources at six sites in the PRD: (a) those in southerly flow, (b) those in

537 northerly flow.



538

539

540

541

542

543

544

545

546

547

548

549

550

551

552

553

554

555

556

557

558

559

560

561

562

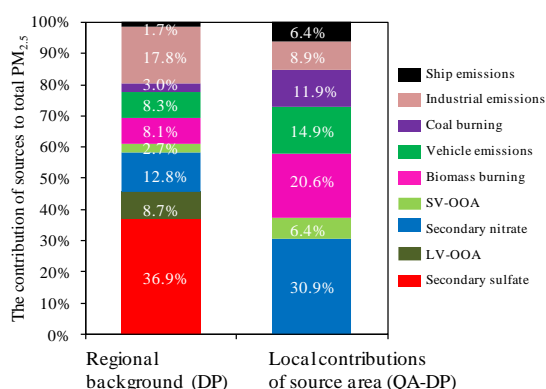
563

Fig. 9. The schematic diagram of high-emission areas in the PRD (map from Google Earth). The white shaded area indicates the key emission area for the multiple sources of SO₂, NO_x, coal burning, biomass burning, industrial emissions and vehicle emissions, and is explained further in the text.

3.5 Distinguishing local and regional PM_{2.5} pollution in the PRD

The analyses presented in Section 3.4 indicate that the secondary sulfates at the four southern coastal sites (DM, QA, UT and DP) in the PRD were almost entirely derived from the conversion of SO₂ from the emissions of ships in the southern ocean during southerly flow, contributing approximately 20% of the average PM_{2.5} (13 μg/m³) at the four sites. Considering that the ship emissions directly contributed approximately 10% of the average PM_{2.5} at the four sites, the total ship emissions contributed approximately 30% of PM_{2.5} in the southern coastal PRD area and acted as the largest source of PM_{2.5}. Under northerly flow conditions, the background DP site, which was barely affected by pollution emissions within the PRD, reflected regional transport from the north air mass outside the PRD, while the background QA site reflected the superposition effect of regional background pollution and the input of the most serious pollution area in the PRD. The consistency of the secondary sulfate concentrations at the background QA and DP sites was interpreted to reflect almost the same regional background effect during northerly flow; thus, the differences in the six anthropogenic sources between the two background sites, including secondary nitrate (and SV-OOA), biomass burning, industrial emissions, coal burning, vehicle emissions and ship emissions, could be used to trace the internal inputs from the most serious pollution area within the PRD to the downwind area. The internal inputs of six anthropogenic sources to the corresponding sources of PM_{2.5} at the background QA site were 66%, 67%, 28%, 76%, 59% and 75%, respectively, and the total internal input of 37.7 μg/m³ accounted for 45% of PM_{2.5} at the background QA site (83 μg/m³), showing that the local contributions of anthropogenic pollution emissions in the key source area of the PRD were still crucial in winter but lower than the contribution of the regional background. Ignoring natural sources, such as aged sea salt and

564 fugitive dust, under northerly flow, the contributions of other anthropogenic sources to DP were
 565 considered to represent regional background pollution ($47.5 \mu\text{g}/\text{m}^3$), and the differences in their
 566 corresponding source concentrations between QA and DP were expected to represent the local
 567 emissions of source areas in the PRD. Therefore, the source structures in the regional background
 568 air mass and local emissions of heavy pollution sources area in the PRD are shown in Fig. 10.
 569 Secondary sulfate and LV-OOA occupied the vast majority (45.6%) of the regional background air
 570 mass from the northern mainland, followed by industrial emissions (17.8%), secondary nitrate and
 571 SV-OOA (15.5%). However, the major sources between the sources output by local emissions
 572 from the heavy pollution source area of the PRD were secondary nitrate and SV-OOA (37.3%),
 573 biomass burning (20.6%), vehicle emissions (14.9%) and coal burning (11.9%). Therefore,
 574 measures implemented for the effective control of $\text{PM}_{2.5}$ in the PRD should focus on local controls
 575 and regional joint prevention and control under winter northerly flow conditions.



576
 577 **Fig. 10.** The $\text{PM}_{2.5}$ source structures in regional background air and local contributions of the central PRD area
 578 under northerly flow.

580 4 Conclusions

581 The PRD is one of the largest agglomeration of cities in the world, and its air quality has
 582 largely improved in the past ten years. To reveal the current $\text{PM}_{2.5}$ pollution characteristics on a
 583 regional scale in the PRD, six sampling sites were selected to conduct four months (one for each
 584 season) of sampling and chemical analysis in 2015; then, the source exploration of $\text{PM}_{2.5}$ was
 585 performed using a novel method. The conclusions are described below.

586 (1) The 4-month average $\text{PM}_{2.5}$ concentration for all six sites in the PRD was $37 \mu\text{g}/\text{m}^3$, of which
 587 OM, SO_4^{2-} , NH_4^+ , NO_3^- , EC, metal elements and Cl^- contributed 36.9%, 23.6%, 10.9%, 9.3%,
 588 6.6%, 6.5% and 0.9%, respectively. The tempo-spatial $\text{PM}_{2.5}$ variations were generally
 589 characterized as being higher in the north inland region and higher in winter.

590 (2) This study revealed that the ME-2 model produced more environmentally meaningful and
 591 statistically robust results of source apportionment than the traditional PMF model. Secondary
 592 sulfate was found to be the dominant source of $\text{PM}_{2.5}$ in the PRD, at 21%, followed by vehicle
 593 emissions (14%), industrial emissions (13%), secondary nitrate (11%), biomass burning (11%),
 594 SOA (7%), coal burning (6%), fugitive dust (5%), ship emissions (3%) and aged sea salt (2%).
 595 Only aged sea salt and ship emissions did not show obvious seasonal variations.

596 (3) Based on the spatial distribution characteristics of $\text{PM}_{2.5}$ sources under typical southerly and
 597 northerly airflow conditions, the central PRD area between MDS, HS and QA is identified as a
 598 key area for source emissions, including SO_2 , NO_x , coal burning, biomass burning, industrial

599 emissions and vehicle emissions, and thus deserves more attention when implementing local
600 pollution control in the PRD. In addition, ship emissions should be controlled more strictly during
601 summer due to its contribution of approximately 30% of PM_{2.5} in the southern coastal area of the
602 PRD under southerly air flow.

603 (4) Under typical winter northerly flow, the contributions of anthropogenic pollution emissions in
604 the central PRD area contributed 37.7 µg/m³ (45% of PM_{2.5}) to the regional background air.
605 Secondary sulfate (36.9%), industrial emissions (17.8%), and secondary nitrate SV-OOA (12.8%)
606 were the major PM_{2.5} sources for the PM_{2.5} transported in the regional background air mass, while
607 secondary nitrate (30.9%), biomass burning (20.6%), vehicle emissions (14.9%) and coal burning
608 (11.9%) were the major sources for the PM_{2.5} produced in the central PRD area. Therefore,
609 effective control measures of PM_{2.5} in the PRD in the future should pay more attention to both
610 local controls and regional joint prevention.

611

612 **Acknowledgments**

613 This work was supported by the National Natural Science Foundation of China (91744202;
614 41622304) and the Science and Technology Plan of Shenzhen Municipality
615 (JCYJ20170412150626172, JCYJ20170306164713148).

616

617 **References**

618 BIPM, IEC, IFCC, ILAC, ISO, IUPAC, IUPAP, and OIML: Evaluation of measurement data -- Guide
619 to the expression of uncertainty in measurement,
620 https://www.bipm.org/utls/common/documents/jcgm/JCGM_100_2008_E.pdf , 2008.

621 Bressi, M., Sciare, J., Gherzi, V., Bonnaire, N., Nicolas, J. B., Petit, J. E., Moukhtar, S., Rosso, A.,
622 Mihalopoulos, N., Féron, A.: A one-year comprehensive chemical characterisation of fine aerosol
623 (PM_{2.5}) at urban, suburban and rural background sites in the region of Paris (France), *Atmos. Chem.*
624 *Phys.*, 15, 7825-7844, doi: 10.5194/acp-13-7825-2013, 2013.

625 Burnett, R. T., Pope, C. A. I., Ezzati, M., Olives, C., Lim, S. S., Mehta, S., Shin, H. H., Singh, G.,
626 Hubbell, B., Brauer, M., Anderson, H. R., Smith, K. R., Balmes, J. R., Bruce, N. G., Kan, H., Laden,
627 F., Prüss-Ustün, A., Turner, M. C., Gapstur, S. M., Diver, W. R., and Cohen, A.: An Integrated Risk
628 Function for Estimating the Global Burden of Disease Attributable to Ambient Fine Particulate
629 Matter Exposure, *Environ. Health Persp.*, 122, A235-A235, doi: 10.1289/ehp.122-A235, 2014.

630 Canonaco, F., Crippa, M., Slowik, J. G., Baltensperger, U., and Prévôt, A. S. H.: SoFi, an IGOR-based
631 interface for the efficient use of the generalized multilinear engine (ME-2) for the source
632 apportionment: ME-2 application to aerosol mass spectrometer data, *Atmos. Meas. Tech.*, 6,
633 3649-3661, doi: 10.5194/amt-6-3649-2013, 2013.

634 Cao, L. M., Huang, X. F., Li, Y. Y., Hu, M., and He, L. Y.: Volatility measurement of atmospheric
635 submicron aerosols in an urban atmosphere in southern China, *Atmos. Chem. Phys.*, 18, 1729-1743,
636 doi: 10.5194/acp-18-1729-2018, 2018.

637 Cho, S. H., Kim, P. R., Han, Y. J., Kim, H. W., and Yi, S. M.: Characteristics of Ionic and
638 Carbonaceous Compounds in PM_{2.5} and High Concentration Events in Chuncheon, Korea, *J. Korean*
639 *Soc. Atmos. Environ.*, 32, 435-447, doi: 10.5572/KOSAE.2016.32.4.435, 2016.

640 Chow, J. C., and Watson, J. G.: Review of PM_{2.5} and PM₁₀ Apportionment for Fossil Fuel Combustion
641 and Other Sources by the Chemical Mass Balance Receptor Model, *Energ. Fuel.*, 16, 222-260, doi:
642 10.1021/ef0101715, 2002.

643 Chow, J. C., Watson, J. G., Pritchett, L. C., Pierson, W. R., Frazier, C. A., and Purcell, R. G.: The DRI
644 thermal/optical reflectance carbon analysis system: description, evaluation and applications in U.S.
645 Air quality studies, *Atmos. Environ.*, 27, 1185-1201, doi: 10.1016/0960-1686(93)90245-T, 1993.

646 Crippa, M., Canonaco, F., Lanz, V. A., Ajä M., Allan, J. D., Carbone, S., Capes, G., Ceburnis, D.,
647 Dall'Osto, M., Day, D. A., DeCarlo, P. F., Ehn, M., Eriksson, A., Freney, E., Hildebrandt Ruiz, L.,
648 Hillamo, R., Jimenez, J. L., Junninen, H., Kiendler-Scharr, A., Kortelainen, A. M., Kulmala, M.,
649 Laaksonen, A., Mensah, A. A., Mohr, C., Nemitz, E., O'Dowd, C., Ovadnevaite, J., Pandis, S. N.,
650 Petä T., Poulain, L., Saarikoski, S., Sellegri, K., Swietlicki, E., Tiitta, P., Worsnop, D. R.,
651 Baltensperger, U., and Prévôt, A. S. H.: Organic aerosol components derived from 25 AMS data sets
652 across Europe using a consistent ME-2 based source apportionment approach, *Atmos. Chem. Phys.*,
653 14, 6159-6176, doi: 10.5194/acp-14-6159-2014, 2014.

654 Elser, M., Huang, R., Wolf, R., Slowik, J. G., Wang, Q., Canonaco, F., Li, G., Bozzetti, C.,
655 Daellenbach, K. R., Huang, Y., Zhang, R., Li, Z., Cao, J., Baltensperger, U., El-Haddad, I., and
656 Prévôt, A. S. H.: New insights into PM_{2.5} chemical composition and sources in two major cities in
657 China during extreme haze events using aerosol mass spectrometry, *Atmos. Chem. Phys.*, 16,
658 3207-3225, doi: 10.5194/acp-16-3207-2016, 2016.

659 Environmental Protection Agency of Jiangmen City: Key pollution sources basic information in
660 Jiangmen, http://hbj.jiangmen.gov.cn/thirdData/hbsjzx/hjjc/fs/201712/t20171218_268676.html,
661 2017.

662 Fröhlich, R., Crenn, V., Setyan, A., Belis, C. A., Canonaco, F., Favez, O., Riffault, V., Slowik, J. G.,
663 Aas, W., Ajä M., Alastuey, A., Artiñano, B., Bonnaire, N., Bozzetti, C., Bressi, M., Carbone, C.,
664 Coz, E., Croteau, P. L., Cubison, M. J., Esser-Gietl, J. K., Green, D. C., Gros, V., Heikkinen, L.,
665 Herrmann, H., Jayne, J. T., Lunder, C. R., Minguillón, M. C., Močnik, G., O'Dowd, C. D.,
666 Ovadnevaite, J., Petralia, E., Poulain, L., Priestman, M., Ripoll, A., Sarda-Estève, R., Wiedensohler,
667 A., Baltensperger, U., Sciare, J., and Prévôt, A. S. H.: ACTRIS ACSM intercomparison – Part 2:
668 Intercomparison of ME-2 organic source apportionment results from 15 individual, co-located
669 aerosol mass spectrometers, *Atmos. Meas. Tech.*, 8, 2555-2576, doi: 10.5194/amt-8-2555-2015,
670 2015.

671 Gao, B., Guo, H., Wang, X., Zhao, X., Ling, Z., Zhang, Z., and Liu, T.: Tracer-based source
672 apportionment of polycyclic aromatic hydrocarbons in PM_{2.5} in Guangzhou, southern China, using
673 positive matrix factorization (PMF), *Environ. Sci. Pollut. R.*, 20, 2398-2409, doi:
674 10.1007/s11356-012-1129-0, 2013.

675 Guangzhou Environmental Protection Bureau: The Results of Source apportionment on PM_{2.5} in
676 Guangzhou in 2016,
677 <http://www.gz.gov.cn/gzgov/s5837/201706/1dcb25be6dd14dc6ab6506e0a5383745.shtml>, 2017.

678 Guangzhou Municipal People's Government: Three-year Action Plan for the Construction of
679 Guangzhou International Shipping Center (2015-2017),
680 <http://www.gz.gov.cn/gzgov/s2811/201509/19601daa69c84e439fe2fb8baea448bb.shtml>, 2015.

681 Hagler, G., Bergin, M., Salmon, L., Yu, J., Wan, E., Zheng, M., Zeng, L., Kiang, C., Zhang, Y., and
682 Lau, A.: Source areas and chemical composition of fine particulate matter in the Pearl River Delta
683 region of China, *Atmos. Environ.*, 40, 3802-3815, doi: 10.1016/j.atmosenv.2006.02.032, 2006.

684 Hasheminassab, S., Daher, N., Ostro, B. D., and Sioutas, C.: Long-term source apportionment of
685 ambient fine particulate matter (PM_{2.5}) in the Los Angeles Basin: A focus on emissions reduction
686 from vehicular sources, *Environ. Pollut.*, 193, 54-64, doi: 10.1016/j.envpol.2014.06.012, 2014.

687 He, L., Huang, X., Xue, L., Hu, M., Lin, Y., Zheng, J., Zhang, R., and Zhang, Y.: Submicron aerosol
688 analysis and organic source apportionment in an urban atmosphere in Pearl River Delta of China
689 using high-resolution aerosol mass spectrometry, *J. Geophys. Res.-Atmos.*, 116, doi:
690 10.1029/2010JD014566, 2011.

691 Hong Kong Marine Department: Ranking of container ports of the world,
692 https://www.mardep.gov.hk/hk/publication/pdf/portstat_2_y_b5c.pdf, 2012.

693 Hu, Z. Y.: Studies on the Discharging and Distribution of Heavy Metal Pollution in the Pearl River
694 Delta, Doctoral dissertation, Graduate School of the Chinese Academy of Sciences (Guangzhou
695 Institute of Geochemistry), 2004.

696 Huang, R., Zhang, Y., Bozzetti, C., Ho, K., Cao, J., Han, Y., Daellenbach, K. R., Slowik, J. G., Platt, S.
697 M., Canonaco, F., Zotter, P., Wolf, R., Pieber, S. M., Bruns, E. A., Crippa, M., Ciarelli, G.,
698 Piazzalunga, A., Schwikowski, M., Abbaszade, G., Schnelle-Kreis, J., Zimmermann, R., An, Z.,
699 Szidat, S., Baltensperger, U., Haddad, I. E., and Prévôt, A. S. H.: High secondary aerosol
700 contribution to particulate pollution during haze events in China, *Nature*, 514, 218-222, doi:
701 10.1038/nature13774, 2014a.

702 Huang, X.F., He, L. Y., Hu, M., Canagaratna, M. R., Kroll, J. H., Ng, N. L., Zhang, Y. H., Lin, Y.,
703 Xue, L., Sun, T. L., Liu, X. G., Shao, M., Jayne, J. T., Worsnop, D. R. Characterization of submicron
704 aerosols at a rural site in Pearl River Delta of China using an Aerodyne High-Resolution Aerosol
705 Mass Spectrometer. *Atmos. Chem. Phys.*, 11(5), 1865–1877, 2011.

706 Huang, X. F., Hui, Y., Gong, Z. H., Xiang, L., He, L. Y., Zhang, Y. H., and Min, H.: Source
707 apportionment and secondary organic aerosol estimation of PM_{2.5} in an urban atmosphere in China,
708 *Sci. China Earth Sci.*, 57, 1352-1362, doi: 10.1007/s11430-013-4686-2, 2014b.

709 Huang, X., Liu, Z., Liu, J., Hu, B., Wen, T., Tang, G., Zhang, J., Wu, F., Ji, D., and Wang, L.:
710 Chemical characterization and source identification of PM_{2.5} at multiple sites in the
711 Beijing-Tianjin-Hebei region, China, *Atmos. Chem. Phys.*, 17, 12941-12962, doi:
712 10.5194/acp-17-12941-2017, 2017.

713 Huang, X., Yu, J. Z., He, L., and Yuan, Z.: Water-soluble organic carbon and oxalate in aerosols at a
714 coastal urban site in China: Size distribution characteristics, sources, and formation mechanisms, *J.*
715 *Geophys. Res.-Atmos.*, 111, doi: 10.1029/2006JD007408, 2006.

716 Jimenez, J. L., Canagaratna, M. R., Donahue, N. M., Prevot, A. S., Zhang, Q., Kroll, J. H., Decarlo, P.
717 F., Allan, J. D., Coe, H., and Ng, N. L.: Evolution of organic aerosols in the atmosphere, *Science*,
718 326, 1525-1529, doi: 10.1126/science.1180353, 2009.

719 Kuang, B. Y., Lin, P., Huang, X. H. H., and Yu, J. Z.: Sources of humic-like substances in the Pearl
720 River Delta, China: positive matrix factorization analysis of PM_{2.5} major components and source
721 markers, *Atmos. Chem. Phys.*, 15, 1995-2008, doi: 10.5194/acp-15-1995-2015, 2015.

722 Lanz, V. A., Alfarra, M. R., Baltensperger, U., Buchmann, B., Hueglin, C., and Prévôt, A. S. H.:
723 Source apportionment of submicron organic aerosols at an urban site by factor analytical modelling
724 of aerosol mass spectra, *Atmos. Chem. Phys.*, 7, 1503-1522, doi: 10.5194/acp-7-1503-2007, 2007.

725 Leiva, M. A., Araya, M. C., Alvarado, A. M., and Seguel, R. J.: Uncertainty estimation of anions and
726 cations measured by ion chromatography in fine urban ambient particles (PM_{2.5}), *Accredit. Qual.*
727 *Assur.*, 17, 53-63, doi: 10.1007/s00769-011-0844-4, 2012.

728 Lelieveld, J., Evans, J. S., Fnais, M., Giannadaki, D., and Pozzer, A.: The contribution of outdoor air
729 pollution sources to premature mortality on a global scale, *Nature*, 525, 367-371, doi:
730 10.1038/nature15371, 2015.

731 Liu, J., Li, J., Zhang, Y., Liu, D., Ding, P., Shen, C., Shen, K., He, Q., Ding, X., and Wang, X.: Source
732 apportionment using radiocarbon and organic tracers for PM_{2.5} carbonaceous aerosols in Guangzhou,
733 South China: contrasting local- and regional-scale haze events, *Environ. Sci. Technol.*, 48, 12002,
734 doi: 10.1021/es503102w, 2014.

735 Mason, B., *Principles of Geochemistry*, 2nd edition, John Wiley and Sons, 1982.

736 Ming, L., Jin, L., Li, J., Fu, P., Yang, W., Liu, D., Zhang, G., Wang, Z., and Li, X.: PM_{2.5} in the
737 Yangtze River Delta, China: Chemical compositions, seasonal variations, and regional pollution
738 events, *Environ. Pollut.*, 223, 200-212, doi: 10.1016/j.envpol.2017.01.013, 2017.

739 Ministry of Ecology and Environment (MEE): Ambient Air-Determination of the water soluble anions
740 (F⁻、Cl⁻、Br⁻、NO₂⁻、NO₃⁻、PO₄³⁻、SO₃²⁻、SO₄²⁻) from atmospheric particles-Ion chromatography
741 (HJ 799-2016), http://kjs.mep.gov.cn/hjbhzbz/bzwb/jcffbz/201605/t20160519_337906.shtml, 2016a.

742 Ministry of Ecology and Environment (MEE): Ambient air-Determination of the water soluble
743 cations(Li⁺、Na⁺、NH₄⁺、K⁺、Ca²⁺、Mg²⁺) from atmospheric particles-Ion chromatography (HJ
744 800-2016), http://kjs.mep.gov.cn/hjbhzbz/bzwb/jcffbz/201605/t20160519_337907.shtml, 2016b.

745 Ministry of Ecology and Environment (MEE): Ambient air and stationary source emission -
746 Determination of metals in ambient particulate matter - Inductively coupled plasma / mass
747 spectrometry (ICP-MS) (HJ 657-2013),
748 http://kjs.mep.gov.cn/hjbhzbz/bzwb/jcffbz/201308/t20130820_257714.shtml, 2013a.

749 Ministry of Ecology and Environment (MEE): Technical Specifications for gravimetric measurement
750 methods for PM_{2.5} in ambient air (HJ 656-2013),
751 http://kjs.mep.gov.cn/hjbhzbz/bzwb/jcffbz/201308/t20130802_256857.shtml, 2013b.

752 Ministry of Environmental Protection: Report on the State of the Environment in China 2015,
753 <http://www.zhb.gov.cn/hjzl/zghjzkgb/lzghjzkgb/201606/P020160602333160471955.pdf>, 2016.

754 Norris, G., and Duvall, R.: EPA Positive Matrix Factorization (PMF) 5.0 Fundamentals and user guide,
755 https://www.epa.gov/sites/production/files/2015-02/documents/pmf_5.0_user_guide.pdf, 2014.

756 Nanfang Daily: PM_{2.5} level fluctuations down in PRD region in the past decade,
757 http://epaper.southcn.com/nfdaily/html/2016-01/03/content_7504954.htm, 2016.

758 Paatero, P., and Tapper, U.: Positive matrix factorization: A non - negative factor model with optimal
759 utilization of error estimates of data values, *Environmetrics*, 5, 111-126, doi:
760 10.1002/env.3170050203, 1994.

761 Paatero, P.: The Multilinear Engine—A Table-Driven, Least Squares Program for Solving Multilinear
762 Problems, Including the n-Way Parallel Factor Analysis Model, *J. Comput. Graph. Stat.*, 8, 854-888,
763 doi: 10.1080/10618600.1999.10474853, 1999.

764 People's Government of Guangdong Province: Major Pollutants Emission Reduction implementation
765 plan during the 12th Five-year Plan in Guangdong Province,
766 http://zwgk.gd.gov.cn/006939748/201212/t20121219_359131.html, 2012.

767 People's Government of Shenzhen Municipality: Air quality improvement plan in Shenzhen,
768 http://zwgk.gd.gov.cn/007543382/201309/t20130930_407564.html, 2013.

769 Physick, W. L., and Goudey, R.: Estimating an annual-average RSP concentration for Hong Kong
770 using days characteristic of the dominant weather patterns, *Atmos. Environ.*, 35, 2697-2705, doi:
771 10.1016/S1352-2310(00)00413-1, 2001.

772 Polissar, A. V., Hopke, P. K., Paatero, P., Malm, W. C., and Sisler, J. F.: Atmospheric aerosol over
773 Alaska: 2. Elemental composition and sources, *J. Geophys. Res.-Atmos.*, 103, 19045 - 19057, 1998.

774 Reyes-Villegas, E., Green, D. C., Priestman, M., Canonaco, F., Coe, H., Prévôt, A. S. H., and Allan, J.

775 D.: Organic Aerosol source apportionment in London 2013 with ME-2: exploring the solution space
776 with annual and seasonal analysis, *Atmos. Chem. Phys.*, 16, 15545-15559, doi:
777 10.5194/acp-16-15545-2016, 2016.

778 Rodr ́guez, S., Van Dingenen, R., Putaud, J.-P., Dell'Acqua, A., Pey, J., Querol, X., Alastuey, A.,
779 Chenery, S., Ho, K.-F., Harrison, R., Tardivo, R., Scarnato, B., and Gemelli, V.: A study on the
780 relationship between mass concentrations, chemistry and number size distribution of urban fine
781 aerosols in Milan, Barcelona and London, *Atmos. Chem. Phys.*, 7, 2217-2232, doi:
782 10.5194/acp-7-2217-2007, 2007.

783 Sarnat, J. A., Marmur, A., Klein, M., Kim, E., Russell, A. G., Sarnat, S. E., Mulholland, J. A., Hopke, P.
784 K., and Tolbert, P. E.: Fine Particle Sources and Cardiorespiratory Morbidity: An Application of
785 Chemical Mass Balance and Factor Analytical Source-Appportionment Methods, *Environ. Health*
786 *Persp.*, 116, 459-66, doi: 10.1289/ehp.10873, 2008.

787 Tan, J., Duan, J., Ma, Y., He, K., Cheng, Y., Deng, S., Huang, Y., and Si-Tu, S.: Long-term trends of
788 chemical characteristics and sources of fine particle in Foshan City, Pearl River Delta: 2008–2014,
789 *Sci. Total Environ.*, 565, 519-528, doi: 10.1016/j.scitotenv.2016.05.059, 2016.

790 Tao, J., Zhang, L., Cao, J., Zhong, L., Chen, D., Yang, Y., Chen, D., Chen, L., Zhang, Z., Wu, Y., Xia,
791 Y., Ye, S., and Zhang, R.: Source apportionment of PM_{2.5} at urban and suburban areas of the Pearl
792 River Delta region, south China - With emphasis on ship emissions, *Sci. Total Environ.*, 574,
793 1559-1570, doi: 10.1016/j.scitotenv.2016.08.175, 2017.

794 Taylor, S. R., and McLennan, S. M.: The geochemical evolution of the continental crust, *Rev. Geophys.*,
795 33, 293-301, doi: 10.1029/95RG00262, 1995.

796 Ulbrich, I. M., Canagaratna, M. R., Zhang, Q., Worsnop, D. R., and Jimenez, J. L.: Interpretation of
797 organic components from Positive Matrix Factorization of aerosol mass spectrometric data, *Atmos.*
798 *Chem. Phys.*, 9, 2891-2918, doi: 10.5194/acp-9-2891-2009, 2009.

799 Villalobos, A. M., Barraza, F., Jorquera, H., and Schauer, J. J.: Chemical speciation and source
800 apportionment of fine particulate matter in Santiago, Chile, 2013, *Sci. Total Environ.*, 512-513,
801 133-142, doi: 10.1016/j.scitotenv.2015.01.006, 2015.

802 Visser, S., Slowik, J. G., Furger, M., Zotter, P., Bukowiecki, N., Canonaco, F., Flechsig, U., Appel, K.,
803 Green, D. C., Tremper, A. H., Young, D. E., Williams, P. I., Allan, J. D., Coe, H., Williams, L. R.,
804 Mohr, C., Xu, L., Ng, N. L., Nemitz, E., Barlow, J. F., Halios, C. H., Fleming, Z. L., Baltensperger,
805 U., and Pr ́v ́t, A. S. H.: Advanced source apportionment of size-resolved trace elements at multiple
806 sites in London during winter, *Atmos. Chem. Phys.*, 15, 11291-11309, doi:
807 10.5194/acp-15-11291-2015, 2015.

808 Wang, H., Tian, M., Chen, Y., Shi, G., Liu, Y., Yang, F., Zhang, L., Deng, L., Yu, J., and Peng, C.:
809 Seasonal characteristics, formation mechanisms and source origins of PM_{2.5} in two megacities in
810 Sichuan Basin, China, *Atmos. Chem. Phys.*, 18, 865-881, doi: 10.5194/acp-18-865-2018, 2018.

811 Wang, J., Ho, S. S. H., Ma, S., Cao, J., Dai, W., Liu, S., Shen, Z., Huang, R., Wang, G., and Han, Y.:
812 Characterization of PM_{2.5} in Guangzhou, China: uses of organic markers for supporting source
813 apportionment, *Sci. Total Environ.*, 550, 961-971, doi: 10.1016/j.scitotenv.2016.01.138, 2016.

814 Wang, Q. Q., Huang, X. H. H., Zhang, T., Zhang, Q., Feng, Y., Yuan, Z., Wu, D., Lau, A. K. H., and
815 Yu, J. Z.: Organic tracer-based source analysis of PM_{2.5} organic and elemental carbon: A case study
816 at Dongguan in the Pearl River Delta, China, *Atmos. Environ.*, 118, 164-175, doi:
817 10.1016/j.atmosenv.2015.07.033, 2015.

818 Wang, Q., Feng, Y., Huang, X. H. H., Griffith, S. M., Zhang, T., Zhang, Q., Wu, D., and Yu, J. Z.: Non

819 - polar organic compounds as PM_{2.5} source tracers: Investigation of their sources and degradation in
820 the Pearl River Delta, China, *J. Geophys. Res.-Atmos.*, 121, 11862-11879, doi:
821 10.1002/2016JD025315, 2017.

822 Yamasoe, M. A., Artaxo, P., Miguel, A. H., and Allen, A. G.: Chemical composition of aerosol
823 particles from direct emissions of vegetation fires in the Amazon Basin: water-soluble species and
824 trace elements, *Atmos. Environ.*, 34, 1641-1653, doi: 10.1016/S1352-2310(99)00329-5, 2000.

825 Yuan, Z., Lau, A., Zhang, H., Yu, J., Louie, P., and Fung, J.: Identification and spatiotemporal
826 variations of dominant PM₁₀ sources over Hong Kong, *Atmos. Environ.*, 40, 1803-1815, doi:
827 10.1016/j.atmosenv.2005.11.030, 2006a.

828 Yuan, Z. B., Yu, J. Z., Lau, A. K. H., Louie, P. K. K., and Fung, J. C. H.: Application of positive
829 matrix factorization in estimating aerosol secondary organic carbon in Hong Kong and its
830 relationship with secondary sulfate, *Atmos. Chem. Phys.*, 6, 25-34, doi: 10.5194/acp-6-25-2006,
831 2006b.

832 Zou, B. B., Huang, X. F., Zhang, B., Dai, J., Zeng, L. W., Feng, N., and He, L. Y.: Source
833 apportionment of PM_{2.5} pollution in an industrial city in southern China, *Atmos. Pollut. Res.*, 8,
834 1193-1202, doi: 10.1016/j.apr.2017.05.001, 2017.